RSC Advances

PAPER

View Article Online
View Journal | View Issue

Cite this: *RSC Adv.*, 2025, **15**, 24122

Recovery of high-quality struvite fertilizer product from swine wastewater using fluidized bed homogeneous crystallization†

The Anh Luu,[a] Gia Cuong Nguyen,[a] Manh Tuan Truong,[a] Van Giang Le *[a] and Xuan Thanh Bui [bc]

Recovering phosphorus (PO_4^{3-}) and nitrogen (NH_4^+) from swine wastewater is critical because their excess release can trigger eutrophication, severely harming aquatic ecosystems. This study introduces a pioneering fluidized-bed homogeneous crystallization (FBHC) process for single-step co-recovery of PO_4^{3-} and NH_4^+. The method ensures compliance with discharge standards and produces a reusable nutrient product. Preliminary jar-test experiments were performed to identify the feasibility of struvite ($MgNH_4PO_4 \cdot 6H_2O$) precipitation and to define the appropriate range for key operational parameters. Subsequently, operational parameters including pH, reaction time, up-flow velocity, cross-sectional loading, and bed height were systematically optimized. Under optimal conditions with a working medium at pH 9, reaction time of 24 min, up-flow velocity of 36 m h^{-1}, cross-sectional loading of 0.27 kg m^{-2} h^{-1}, and bed height of 10 cm, the total removal efficiencies reached 97.42% for PO_4^{3-} and 86.55% for NH_4^+. The corresponding crystallization ratios were 95.55% and 83.18%, respectively. The FBHC process exhibited high crystallization efficiency (>95%), contributing to reduced impurity levels and improved energy efficiency compared to conventional fluidized bed and chemical precipitation methods. The recovered product was identified as high-purity struvite (94.3%), predominantly comprising particles smaller than 0.75 mm. These results demonstrate the effectiveness of the FBHC strategy for simultaneous nutrient removal and resource recovery through the production of a value-added fertilizer.

Received 13th May 2025
Accepted 1st July 2025

DOI: 10.1039/d5ra03370e

rsc.li/rsc-advances

1. Introduction

Untreated pig swine wastewater is rich in nitrogen,[1] phosphorus,[2] and potassium.[3] Releasing this untreated waste poses a significant threat to soil and water quality. Elevated levels of nitrogen and phosphorus, for instance, can lead to eutrophication in water bodies like rivers and lakes. Furthermore, various forms of nitrogen (such as ammonium, nitrate, and nitrite) and phosphorus (including orthophosphate and monophosphate) present in the wastewater can be toxic to aquatic life.[4] Global consumption of phosphate rock has been steadily increasing, reaching approximately 44.5 million tonnes in 2016,[5] various industrial and human waste streams contain substantial amounts of inorganic phosphate. For instance, dairy wastewater can have 19–445 mg L^{-1},[6,7] swine wastewater 100–453 mg L^{-1},[8,9] urine 20–328 mg L^{-1},[10] and anodized wastewater a striking 3240–9937 mg L^{-1}.[11] Struvite, also known as magnesium ammonium phosphate hexahydrate with the chemical formula $MgNH_4PO_4 \cdot 6H_2O$, is a valuable fertilizer derived from phosphate removal processes. Its increasing popularity in these systems highlights its role in resource recovery and the circular economy by capturing phosphate from agricultural and livestock wastewater and repurposing it as a fertilizer for agricultural use.[12]

Various recovery methods, such as electrodialysis,[13] electrochemical stripping,[14] fluidized bed reactors (FBR),[15,16] ion exchange adsorbents,[17] precipitation, and absorption,[18] have been implemented to treat swine wastewater. Current technological efforts are primarily focused on the recovery of nitrogen and phosphorus.[19] Among these, conventional chemical precipitation is widely recognized as an effective method for phosphorus reclamation in the form of struvite, owing to its ability to generate valuable by-products with high recovery efficiency and minimal environmental impact.[20] Nevertheless, this method produces substantial quantities of sludge, necessitating additional settling units due to its limited efficiency in physically separating the struvite product.[21] Moreover, the resulting sludge, being very wet, needs to undergo a drying step

[a]*Central Institute for Natural Resources and Environmental Studies, Vietnam National University, Hanoi, 111000, Vietnam. E-mail: levangiangcres@vnu.edu.vn*

[b]*Key Laboratory of Advanced Waste Treatment Technology, Ho Chi Minh City University of Technology (HCMUT), Vietnam National University Ho Chi Minh (VNU-HCM), Thu Duc City, Ho Chi Minh City 700000, Vietnam*

[c]*Faculty of Environment and Natural Resources, Ho Chi Minh City University of Technology (HCMUT), 268 Ly Thuong Kiet Street, District 10, Ho Chi Minh City 700000, Vietnam*

† Electronic supplementary information (ESI) available. See DOI: https://doi.org/10.1039/d5ra03370e

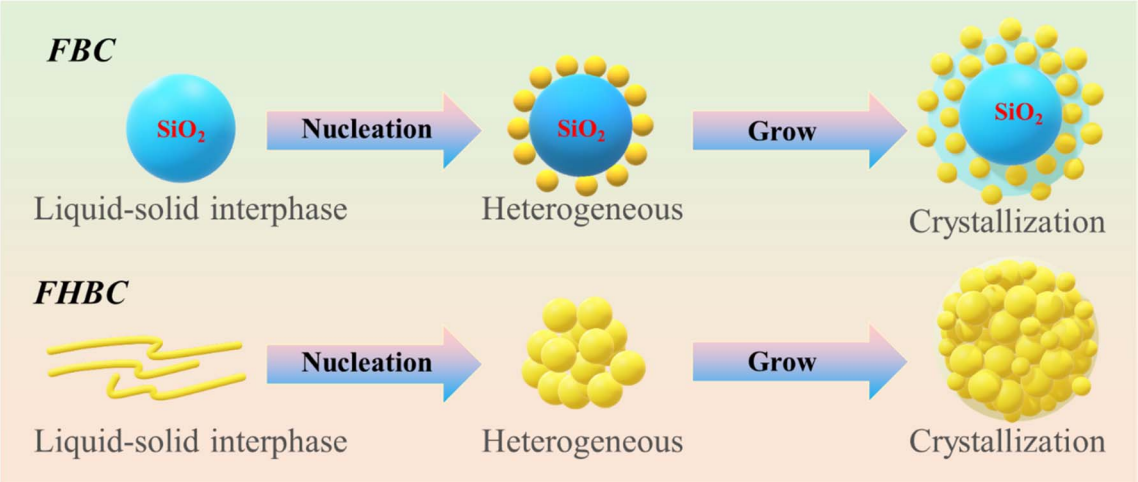

Scheme 1 Mechanisms of the heterogeneous and homogeneous nucleation in FBC and FBHC.

afterward. Nitrogen recovery often involves a stripping process. In this method, ammonia gas (NH_3) is captured by adsorption onto phosphorous acid. This step prepares the nitrogen for a later precipitation reaction with magnesium, ultimately yielding magnesium potassium phosphate hexahydrate ($MgKPO_4 \cdot 6H_2O$). Nonetheless, this stripping technique is not very efficient when it comes to recovering phosphorus.

The fluidized-bed crystallization (FBC) method enables the recovery of pollutants as solid crystals or granules[22,23] (Scheme 1). By introducing magnesium (Mg) or calcium (Ca), phosphorus (P) and nitrogen (N) can be captured as ternary compounds like trimagnesium phosphate 22-hydrate ($Mg_3(PO_4)_2 \cdot 22H_2O$), magnesium ammonium phosphate hexahydrate ($MgNH_4PO_4 \cdot 6H_2O$), and trimagnesium phosphate octahydrate ($Mg_3(PO_4)_2 \cdot 8H_2O$).[24,25] This FBC process enhances precipitation efficiency, using fewer chemicals and minimizing water-rich sludge by forming low-moisture pellets suitable as slow-release fertilizers. However, the process necessitates seeding materials such as silica or aluminum oxide, which can introduce impurities into the final pellets. To overcome this issue of impurity introduction from seed materials in FBC, a seedless fluidized-bed homogeneous crystallization (FBHC) system could be a potential solution. FBHC offers improved separation, purer granules, and faster settling.[26,27] Furthermore, regulating the water flow within the FBHC system facilitates the formation of granular pellets and reduces the generation of wet sludge.[28] Therefore, the FBHC reactor can generate a stable form of magnesium ammonium phosphate hexahydrate, known as struvite ($MgNH_4PO_4 \cdot 6H_2O$), which has a very low solubility product constant (K_{sp}) of 7.08×10^{-14} at 25 °C.[29]

Due to its high organic content and the presence of calcium ions and other impurities in swine wastewater, this matrix presents significant challenges in controlling the crystallization process and achieving high recovery efficiency. Therefore, this study was conducted to initially determine the optimal crystallization conditions through jar-test experiments, and subsequently develop and optimize a FBHC process to simultaneously recover nitrogen (NH_4^+) and phosphorus (PO_4^{3-}) from swine wastewater. By investigating the effects of operating parameters such as pH, reaction time, up-flow velocity, cross-sectional loading, and particle bed height, the study is expected to identify the optimal conditions for effective struvite crystallization. The outcomes are expected to enhance livestock wastewater treatment technologies while producing high-value, reusable fertilizer products, thereby supporting sustainable agricultural practices and promoting a circular economy.

2. Materials and methods

2.1. Materials

Swine wastewater was collected from a pig farm located in Hanoi City, Vietnam and stored at 5.0 ± 1 °C. Before use, actual swine wastewater was filtered (0.45 μm, Whatman) to remove the suspended solids. The properties of the swine wastewater utilized in the experiments are detailed in Table 1.

The chemicals used in this study, including calcium chloride dihydrate ($CaCl_2 \cdot 2H_2O$, 96%), potassium chloride (KCl, 99%),

Table 1 The characteristics of filtered actual swine wastewater used in this study

Parameter	Units	Average values plus standard deviation
pH	—	7.14 ± 0.03
COD	mg L^{-1}	3800 ± 230
Alkalinity (as Na_2CO_3)	mg L^{-1}	2030 ± 160
TAN (total ammonia nitrogen)	mg L^{-1}	549 ± 25
T-P (total phosphorus)	mg L^{-1}	149 ± 10.5
PO_4–P	mg L^{-1}	111 ± 8.0
NH_4–N	mg L^{-1}	441 ± 21
K	mg L^{-1}	312 ± 18
Mg	mg L^{-1}	67.4 ± 7.8
Ca	mg L^{-1}	47.5 ± 4.5
Cu	mg L^{-1}	1.3 ± 0.1
Fe	mg L^{-1}	2.2 ± 0.1
Zn	mg L^{-1}	0.8 ± 0.1

magnesium chloride hexahydrate ($MgCl_2 \cdot 6H_2O$, 99%), sodium phosphate monobasic ($NaH_2PO_4 \cdot 2H_2O$, 99%), potassium phosphate monobasic (KH_2PO_4, 99%), and ammonium chloride (NH_4Cl, 99.8%), were all sourced from Sinopharm Chemical Reagent Co., Ltd, and used as received without further purification. High-purity standards (Charleston, U.S.A.) provided the ICP-MS standard solutions. A laboratory-grade RO ultrapure water system supplied deionized water for all experiments with a resistance greater than 18.1 MΩ.

2.2. Analytical methods

A portable pH meter (TS-1, Suntex) equipped with a plastic pH electrode (GB-600E, Yeong-Shin Company) was utilized to determine the pH of the samples. This meter was calibrated weekly under ambient conditions employing pH 7 and pH 10 buffer solutions. The concentrations of cations and anions in liquid samples were quantified using an inductively coupled plasma mass spectrometry (ICP-MS, iCAP RQ, Thermofisher Scientific Pte Ltd, Singapore) at specific detection wavelengths (213.857 nm, 214.915 nm, 220.353 nm, 231.604 nm, 267.716 nm, 279.553 nm, 324.754 nm, 422.673 nm, 438.364 nm, and 766.491 nm). The method detection limits (MDLs) for heavy metals were 0.15 μg L^{-1} for Fe, 1.17 μg L^{-1} for Zn, and 0.07 μg L^{-1} for Cu,[30] ensuring sufficient sensitivity for detecting trace levels in swine wastewater. Ammonium nitrogen (NH_4–N) levels in the influent and effluent of each reactor were measured with a Flow Injection Analyzer (Lachat Instruments 5600) following the SFS-EN ISO 6878 standard method. The crystalline structure of dried precipitates and granules was identified utilizing an X-ray diffractometer (Rigaku RX III, Japan) with CuKα radiation (40 kV, 30 mA), scanning from 10° to 90° in 0.05° steps with a 0.5 s scan time. The elemental composition of solids was analyzed employing an attached Energy Dispersive Spectrometer (LINKS AN10000/85S, Japan). The morphology of the precipitates was visualized utilizing a Scanning Electron Microscope (Hitachi SU8010, Japan) after coating the samples with a thin layer of platinum using a sputter coater (JEOL JFC-1600).

2.3. Jar-tests

While various materials like nano zero-valent iron (nZVI), marble dust, and graphene oxide can eliminate phosphorus through adsorption or precipitation, magnesium salts are commonly preferred owing to their widespread availability and lower initial investment. This study investigated phosphorus precipitation in batch experiments by varying pH (±0.2) (7.0, 8.0, 8.5, 9.0, and 9.5, and 10; $[N]_0$ of 314.7 mg L^{-1}, $[P]_0$ of 1660.6 mg L^{-1}), reaction time (0, 5, 10, 15, 20, 25, 30, 45, 60, 75, 90, 120, and 150 min), and the molar ratio of magnesium to phosphorus (1.0, 1.2, 1.3, 1.5, 1.8, and 2.0), all at a consistent [Mg]/[P] ratio, pH, and reaction time respectively. Additionally, the impact of different ammonia concentrations (200, 250, 300, 350, 400, and 450 ppm) was examined. All batch tests were conducted at room temperature (25–28 °C).

In jar-test experiments, magnesium chloride and sodium dihydrogen phosphate were dissolved and mixed in deionized water. Swine wastewater was then added to initiate precipitation. The pH was adjusted with sodium hydroxide. The mixture was rapidly stirred, then slowly stirred, and finally allowed to settle. Samples were filtered for analysis. The effect of

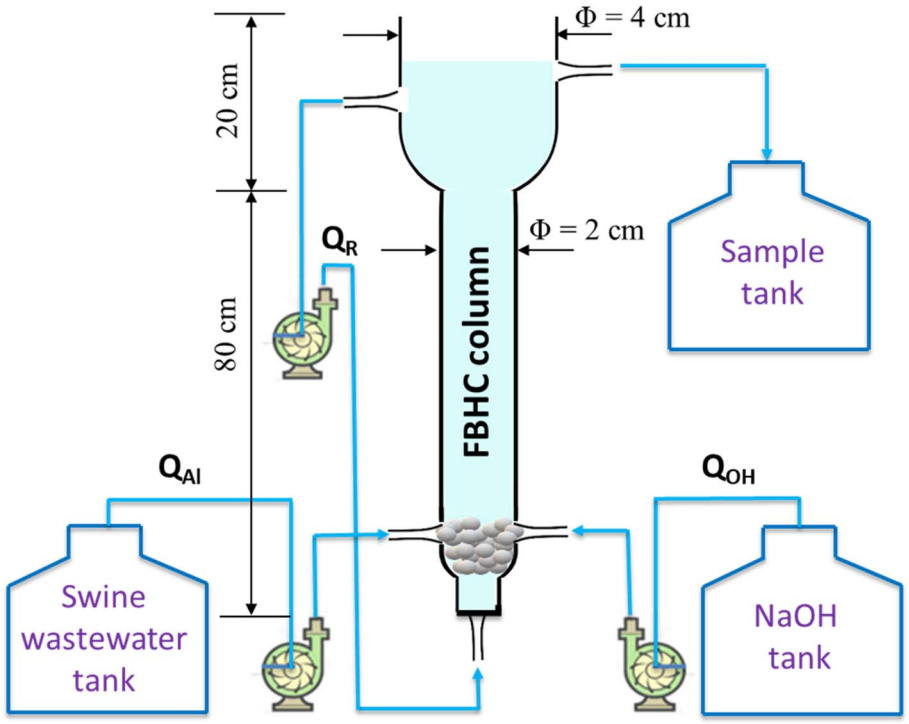

Scheme 2 Schematic of fluidized bed homogeneous crystallization reactor.

ammonium concentration on phosphorus and nitrogen removal was also evaluated by adding ammonium chloride. The key experimental factors explored were pH, reaction time, magnesium-to-phosphorus molar ratios, and ammonium concentrations. All jar-test experiments were performed at 25 °C and replicated.

2.4. Fluidized bed homogeneous crystallization (FBHC)

The fluidized-bed reactor, depicted in Scheme 2, consists of a 550 mL cylindrical column and Pyrex glass pipelines. It's constructed with two sections joined by a wider connection. The lower section has a diameter of 2 cm and a height of 20 cm, while the upper section is 4 cm in diameter and 80 cm high. This widening from top to bottom in the FBC column design helps to decrease the water flow rate and prevent excessive loss of fine particles. Two peristaltic pumps are used to introduce swine wastewater chemicals and sodium hydroxide into the reactor. A third peristaltic pump regulates the recirculation flow rate. To support the granulation bed, ensure even distribution of water flow, facilitate bubble formation at the inlets, and prevent blockages, glass beads with a diameter (D) of 0.5 cm are packed to a height of 3.5 cm from the bottom of both columns. The duration that water remained within the system, known as the hydraulic retention time (HRT), was managed by changing the overall incoming water flow (Q_t) and the rate at which water was cycled back into the system (Q_r).

The pH of the precipitant solutions was adjusted employing either NaOH or HNO_3. The study investigated struvite recovery under varying conditions: pH levels (±0.2) values (8.6, 8.7, 8.8, 8.9, 9.0, 9.1, 9.15, 9.2, 9.3, and 9.4; [Mg]/[P] ratio of 1.2; up-flow

Table 2 Summary of operating parameters of jar-tests and homogeneous fluidized bed reactor

No.	Operational parameters	Jar-tests	FBHC column
1	pH (—)	7.0, 8.0, 8.5, 9.0, 9.5, and 10	8.6, 8.7, 8.8, 8.9, 9.0, 9.1, 9.15, 9.2, 9.3, and 9.4
	[Mg]/[P]	1.0	1.2
	U (m h^{-1})	30	33
	Reaction time (min)	120	60
	L (kg m^{-2} h^{-1})	0.23	0.23
	Bed height (cm)	15	15
	[NH_4^+] (mg L^{-1})	314	—
2	Reaction time (min)	0, 5, 10, 15, 20, 25, 30, 45, 60, 75, 90, 120, and 150	17, 19, 21, 24, 33, and 40
	pH (—)	9.0 ± 0.2	9.0 ± 0.2
	U (m h^{-1})	30	33
	[Mg]/[P]	1.0	1.2
	L (kg m^{-2} h^{-1})	0.23	0.23
	[NH_4^+] (mg L^{-1})	314	—
	Bed height (cm)	15	15
3	[Mg]/[P]	1.0, 1.2, 1.3, 1.5, 1.8, and 2.0	1.2
	U (m h^{-1})	30	33
	pH (—)	9.0 ± 0.1	9.0 ± 0.1
	L (kg m^{-2} h^{-1})	0.23	0.23
	Reaction time (min)	60	24
	[NH_4^+]	314	—
	Bed height (cm)	15	15
4	[NH_4^+]	250, 300, 350, 400, and 450	—
	[Mg]/[P]	1.2	1.2
	pH (—)	9.0 ± 0.1	9.0 ± 0.1
	L (kg m^{-2} h^{-1})	0.23	0.23
	Reaction time (min)	60	24
	Bed height (cm)	15	15
	U (m h^{-1})	30	33
5	U (m h^{-1})	—	14, 18, 22, 26, 29, 33, 36, 40, and 43
	Reaction time (min)	—	24
	[Mg]/[P]	—	1.2
	pH (—)	—	9.0 ± 0.1
	L (kg m^{-2} h^{-1})	—	0.23
	Bed height (cm)	—	15
6	L (kg m^{-2} h^{-1})	—	0.15, 0.19, 0.23, 0.27, 0.31, and 0.34
	Reaction time (min)	—	24
	pH (—)	—	9.0 ± 0.2
	Bed height (cm)	—	15
	U (m h^{-1})		36
7	Bed height (cm)	—	5, 10, 15, 20, 25, and 30
	Reaction time (min)	—	24
	pH (—)	—	9.0 ± 0.2
	U (m h^{-1})	—	36
	L (kg m^{-2} h^{-1})	—	0.27

velocity of 33 m h^{-1}), hydraulic retention time (17, 19, 21, 24, 33, and 40; pH 9 ± 0.2; up-flow velocity of 33 m h^{-1}), different up-flow velocity values (14, 18, 22, 26, 29, 33, 36, 40, and 43 m h^{-1}; pH 9.0 ± 0.2; HRT 24 min), cross-sectional loading (L) (0.15, 0.19, 0.23, 0.27, 0.31, and 0.34 kg m^{-2} h^{-1}; up-flow velocity of 36 m h^{-1}, pH 9 ± 0.2), and bed-height (5, 10, 15, 20, 25, and 30; cross-sectional loading of 0.27 kg m^{-2} h^{-1}, pH 9 ± 0.2, up-flow velocity 36 m h^{-1}) (Table 2).

Scheme 2 visually presents the experimental arrangement for recovering struvite through fluidized bed crystallization. Experiments on the recovery of P and N using the FBHC process were initiated by introducing the feeds of swine wastewater, which was also mixed with NaOH at given flow rates, under room temperature, controlling the ratio of reflux flow (Q_r) to the total inflow ($Q_t = Q_{swine} + Q_{OH}$). Before operating the FBHC reactor, a 3–5 day initial phase was conducted at a low upward flow speed (15 m h^{-1}) to promote granule formation. Subsequently, the upward velocity ($Q_{up} = Q_t + Q_r$) was increased to a superficial velocity of 25 m h^{-1} by regulating the recirculation flow (Q_r). Guided by prior jar-tests results, the reactor was fed with a solution containing magnesium, nitrogen, and phosphorus at a molar ratio of 1.2 (specifically, 402.5 mg-N L^{-1}, 35.2 mg-Mg L^{-1}, and 95.8 mg-P L^{-1}). The FBHC process was run for a duration equivalent to at least nine hydraulic retention times (HRT) to ensure the reaction reached a stable state after any changes to the input conditions.

Effluent samples underwent analysis both with and without filtration utilizing a 0.45 μm filter (GHP Membrane, Pall) to eliminate fine particles. To minimize supersaturation, 1.0 mL of HCl was added to each sample. Soluble nitrogen and phosphorus levels in the filtered samples were used to calculate the overall removal of P and N. Conversely, acidic digestion determined the total P and N content, which was used to assess granulation efficiency.

The removal efficiency was evaluated to assess the capability of the FBHC system to precipitate and recover P and N into granular form, based on the residual concentrations in the effluent. Furthermore, the performance of the jar-test and FBHC processes was quantified by calculating the total recovery (TR) and crystallization ratio (CR) for both phosphorus and nitrogen. Granulation efficiency, on the other hand, was evaluated to confirm the formation of granules with low water content and minimal or no sludge production. The percentage recoveries of P and N were determined using the following calculations in eqn (1) and (2):

$$\mathrm{TR}\ (\%) = \left(1 - \frac{[\mathrm{A}]_s \times Q_t}{C_A \times Q_{(N+P)}}\right) \times 100\% \quad (1)$$

$$\mathrm{CR}\ (\%) = \left(1 - \frac{[\mathrm{A}]_t \times Q_t}{C_A \times Q_{(N+P)}}\right) \times 100\% \quad (2)$$

in which $[A]_s$ represents the amount (in moles) of soluble nitrogen and phosphorus found in the filtered samples (employing a 0.45 μm filter). $[A]_t$ refers to the total nitrogen and phosphorus content obtained after acid digestion of the samples. Q_t represents the overall influent flow rate (in mL min^{-1}), whereas $Q_{(N+P)}$ specifically denotes the influent flow rate of nitrogen and phosphorus ions (in mL min^{-1}). C_A indicates the concentration (in moles) of nitrogen and phosphorus ions in the feed tank. The TR (%) indicated how effectively nitrogen or phosphorus was transformed into solid forms. In contrast, the (CR%) represented the FBHC's ability to retrieve these elements as fluidized crystals. After the experiment, all pellets were collected and sieved to determine the distribution of their sizes.

2.5. Purity of struvite pellets

To determine the purity and composition of the heavy metals in struvite pellets, each sample's 1.5 g was dissolved in 0.5% HNO_3 solution and then diluted with distilled water to 25 mL.[31] Solution pH was adjusted to 4 ± 0.02 by 1.0 M NaOH before analysis. The purity of the struvite was calculated based on the respective N concentrations, calculated by eqn (3):

$$\text{Struvite purity} = \frac{n_N \times M_{struvite}}{m_{struvite}} \times 100\% \quad (3)$$

where n_N denotes the molar amount of N (mol), $M_{struvite}$ refers to the molar mass (g mol^{-1}) of struvite and $m_{struvite}$ represents the mass of the pellets (g).

To analyze how the struvite particles were sized, samples were collected from the bottom of the experimental setup, dried at 50 °C over an 8 hour period, and subsequently separated into distinct size groups utilizing sieves. These groups corresponded to particle diameters of over 2 mm, between 1.4 and 2 mm, between 0.75 and 1.4 mm, between 0.2 and 0.75 mm, and below 0.2 mm. The mass of particles within each size category was then measured to determine the overall size distribution, and the calculations proceeded (eqn (4)) as follows:

$$[\mathrm{Struvite}]_{WF}\ (\%) = \frac{W_{sieve}}{W_{total}} \times 100 \quad (4)$$

where w_{sieve} refers to the weight of pellets greater than the mesh size (g), and w_{total} shows the total weight of the pellets (g).

3. Results and discussion

3.1. Jar-test results

3.1.1. Effect of pH. Fig. 1(a) illustrates the relationship between pH and the removal efficiency of PO_4^{3-} and NH_4^+ ions. The results show that as the pH increases from 7 to 8, the removal efficiency of both ions also tends to increase sharply. Specifically, the CR values of NH_4^+ and PO_4^{3-} increase from 25.33 to 83.75% and 41.09 to 87.32%, respectively. The narrow error bars indicate very low variability between replicates, particularly in the pH range of 7 to 9.5. This demonstrates the high reliability of the results and supports the selection of pH 9 as the optimal condition. Similarly, the TR of NH_4^+ and PO_4^{3-} improved significantly from 28.39 to 82.89% and 43.17 to 89.82%. At a pH greater than 9, no significant fluctuations were observed. While the TR and CR of PO_4^{3-} increased slightly in alkaline conditions, those of NH_4^+ peaked at pH 9 and decreased at pH 9.5 and 10. In the pH range of 11–12, $Mg(OH)_2$ precipitation can potentially interfere with the formation of struvite.[32] Another possibility is that at a very high pH, the

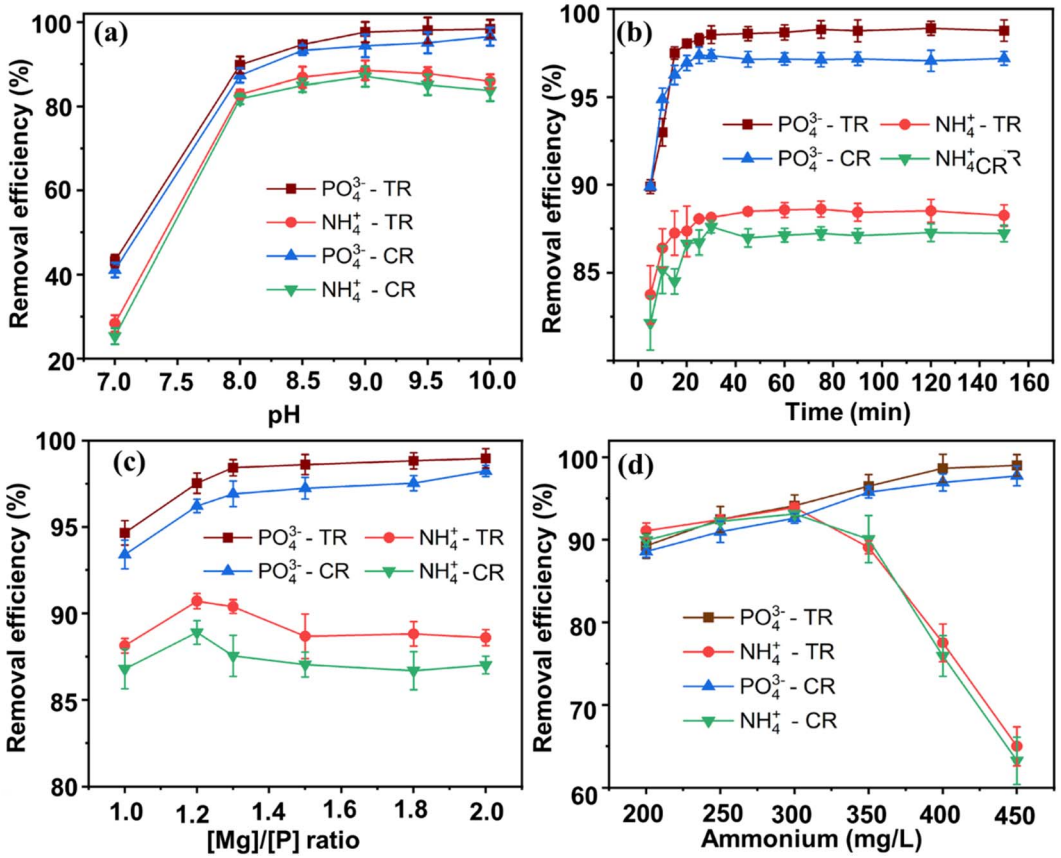

Fig. 1 Effects of (a) pH, (b) reaction time, (c) [Mg]/[P] ratio, and (d) ammonium concentration on TR% and CR%. Error bars represent the standard deviation (±5%) of the replicate experiments.

release of ammonia gas (NH_3) from the solution may occur, reducing the amount of ammonium available for precipitation as struvite.[33,34] The slight difference between the TR and CR curves suggests that crystallization remains the dominant mechanism for ammonium removal within the examined pH range, though minor ammonium loss *via* volatilization may occur at very high pH.

3.1.2. Effect of reaction time. Fig. 1(b) shows the change in removal efficiency with reaction time. In the initial stage (approximately 20 to 40 min), phosphate and ammonium removal efficiency increased rapidly. Subsequently, the removal rate slowed down, reaching a relatively stable state after about 60 to 80 min. The standard deviation of the results is very small, particularly for PO_4^{3-}, indicating high repeatability among replicates. For NH_4^+, although the error is slightly larger at the initial time point (20 min), it stabilizes significantly after 24 min. The removal efficiency of phosphate reached a very high and more stable level than that of ammonium over time. The CR and TR values for PO_4^{3-} were 97.15 and 98.66%, respectively, compared to 87.12 and 88.66% for NH_4^+. The initial rapid increase in removal efficiency may be due to the rapid formation of struvite crystal nuclei, followed by their growth in the fluidized bed. This stage is characterized by a high precipitation reaction rate due to the relatively high concentration of the reactants in the solution. Specifically, Mg^{2+} released from $MgCl_2$ rapidly reacted with Na^+, NH_4^+, and HPO_4^{2-} to form $MgNH_4PO_4 \cdot 6H_2O$ and $MgNaPO_4 \cdot 7H_2O$. Nonetheless, the $MgNaPO_4 \cdot 7H_2O$ might have dissolved as the reaction time prolonged, and the released Mg^{2+} and PO_4^{3-} could have combined to form $Mg_3(PO_4)_2$, resulting in a higher phosphate removal efficiency than ammoniums for most of the reaction duration. Following the rapid growth phase, the elimination rate decelerated and stabilized after approximately 60–80 min, primarily due to the solution's depletion of reactant ions (Mg^{2+}, PO_4^{3-}, and NH_4^+), decreasing the driving force for crystallization.

3.1.3. Effect of [Mg]/[P] ratio. Prior investigations indicate that the dosage of Mg, and P largely determines the extent of nutrient removal. To assess their influence on the removal, various molar ratios of magnesium to phosphorus ([Mg]/[P]) were tested at a pH of 9. Fig. 1(c) shows the effect of the molar ratio of ([Mg]/[P]) on the removal efficiency of PO_4^{3-} and ammonium NH_4^+. It is observed that as the [Mg]/[P] ratio increased from 1.0 to about 1.3, the phosphate removal efficiency (TR and CR) both increased significantly, reaching almost maximum values (about 98.43% for TR and 96.41% for CR). For ammonium, the removal efficiency (for both TR and CR) also tends to increase as the [Mg]/[P] ratio increases from 1.0 to 1.2. However, this increase is less significant compared to phosphate removal, and the achieved values are slightly lower (about 90.7% for TR and 88.9% for CR). These findings suggest that struvite crystallization is favored

even at lower Mg^{2+} levels, thereby promoting the gradual dissolution of magnesium hydroxide ($Mg(OH)_2$) to replenish Mg^{2+} ions for the reaction. This observation can likely be attributed to the dramatically lower solubility product ($K_{sp} = 10^{-13.6}$) of struvite ($MgNH_4PO_4 \cdot 6H_2O$) compared to both Na-struvite ($K_{sp} = 10^{-11.6}$) and K-struvite ($K_{sp} = 10^{-10.6}$),[35] making struvite thermodynamically more preferable for precipitation under similar conditions. Kim *et al.*'s study established an optimal magnesium to phosphorus ([Mg]/[P]) ratio of 1.2 : 1.0, and a practical application at a larger scale suggests a slightly higher ratio of 1.3 : 1.[36] However, further increases in the [Mg]/[P] ratio beyond 1.3 (up to 2) result in only a marginal increase or even a plateau in phosphate removal efficiency, suggesting that the optimal threshold for this ratio has been reached. At higher ratios, the ammonium harvesting efficiency tended to decrease slightly, which can be attributed to the consumption of phosphorus in the process of $Mg_3(PO_4)_2$ formation[36] or a smaller fraction of nitrogen was recovered *via* struvite formation.[37] The stability of $MgRPO_4 \cdot nH_2O$ depends on the ionic radius of *R*.[38] Because Na^+ and K^+ are larger than NH_4^+, their struvite analogs (Na-struvite and K-struvite) exhibit higher stability than NH_4-struvite. Ultimately, although magnesium is required for struvite formation, the optimum [Mg]/[P] ratio for phosphate removal does not exactly coincide with the optimum for ammonium removal, and other factors such as high ammonium initial concentration or crystallization kinetics may be more important in determining ammonium removal efficiency.

3.1.4. Effect of ammonium concentration. Conventional methods for removing ammonium from wastewater include nitrification (around 95% efficiency)[39] and stripping (up to 99% removal).[18,40] Due to the potential influence of ammonium struvite precipitation on phosphorus removal in the presence of substantial ammonium, we conducted jar-tests. These experiments were carried out at a pH of 9, a Mg : P molar ratio of 1.3, and with ammonium levels varying from 200 to 450 mg L^{-1} (Fig. 1(d)). An initial observation shows that both the CR and TR values of PO_4^{3-} and NH_4^+ increase and reach a threshold of 92–93% when the ammonium concentration is 300 mg L^{-1}. Although the ammonium removal efficiency fluctuated at high concentrations, the results from repeated experiments showed small errors and clear changing trends, indicating that the results were reproducible. However, a contrasting trend is evident at higher ammonium concentrations. Specifically, the CR% and TR% for PO_4^{3-} reached approximately 97.72 and 99.01%, respectively, while those for NH_4^+ were significantly lower at only 63.25 and 64.98%. Phosphate removal consistently stayed within the 97–99% range *via* ammonium struvite precipitation, likely because of the creation of non-crystalline substances like $Ca_3(PO_4)_2$ and $Mg_3(PO_4)_2$.[41] Additionally, the production of ammonium struvite was sensitive to pH levels, as previously noted.

3.2. Removal of P and N from swine wastewater by FBHC process

3.2.1. Effect of pH. Fig. 2(a) shows the removal efficiency of PO_4^{3-} and NH_4^+ with pH, discovering that the phosphate removal efficiency (both TR and CR) remained high and exhibited a slight increase as the pH rose from 8.6 to 9.4, exceeding 96%. In contrast, the ammonium removal efficiency was more variable, with TR and CR values generally lower than those of phosphate and showing a tendency to decrease after reaching a peak around pH 9. This difference can likely be attributed to the higher crystallization affinity of phosphate, along with the potential loss of ammonium through volatilization at elevated pH[33] were calculated according to the eqn (5):

$$NH_4^+ + OH^- \rightarrow NH_3 + H_2O,\ K_b = 10^{-4.8} \quad (5)$$

This observation aligns with the work of Çelen and Türker, who similarly found no ammonia loss at pH 7 and a 17.9% loss at pH 9.5.[34] In addition, at high pH, $Mg_3(PO_4)_2$ formation is more favorable,[32] struvite crystals begin to dissolve, releasing Mg^{2+} ions, and $Mg(OH)_2$ precipitation may compete with struvite precipitation.[42] Fig. 2(b) illustrates the residual concentrations of phosphate and ammonium, respectively, showing that the residual phosphate concentration decreased as the phosphate removal efficiency increased, while the residual ammonium concentration fluctuated and showed a tendency to rise again at higher pH values, consistent with the trend observed in ammonium removal efficiency. The recovery efficiency values between replicates varied within a narrow range, especially for phosphorus, reflecting the stability and reliability of the FBHC system when operating at different pH values. Overall, the results indicated that a slightly alkaline pH was beneficial for phosphate removal, but excessively high pH levels could negatively impact NH_4^+ removal. Therefore, a pH of 9 was selected for subsequent experiments.

3.2.2. Effect of hydraulic retention time. Fig. 2(c) illustrates how varying the retention time influences the removal of struvite from swine wastewater. It is observed that the TR of PO_4^{3-} reached a maximum value of approximately 96.52% at HRT 24 min, then tended to decrease slightly as HRT increased. The CR of PO_4^{3-} also showed a similar trend, reaching a maximum of about 93.18% at HRT 24 min. For NH_4^+, both CR and TR increased with increasing HRT from 15 to 24 min, after which they showed a slight decrease. It is noteworthy that the phosphate removal efficiency was consistently and significantly higher than the ammonium removal efficiency across all examined HRT values. This can be attributed to the higher affinity of phosphate for metal ions, such as magnesium (commonly found in swine wastewater), compared to ammonium during struvite crystallization ($MgNH_4PO_4 \cdot 6H_2O$). In the initial stage, rapid reactions between Mg^{2+}, PO_4^{3-}, and NH_4^+ dominate, forming struvite nuclei (eqn (6)):

$$Mg^{2+} + NH_4^+ + PO_4^{3-} + 6H_2O \rightarrow MgNH_4PO_4 \cdot 6H_2O \quad (6)$$

Simultaneously, the intermediate phase like newberyite ($MgHPO_4 \cdot 3H_2O$) which later transform into struvite in the occurrence of PO_4^{3-} and NH_4^+ (eqn (7)):

$$MgHPO_4 \cdot 3H_2O + NH_4^+ + 3H_2O \rightarrow MgNH_4PO_4 \cdot 6H_2O + H^+ \quad (7)$$

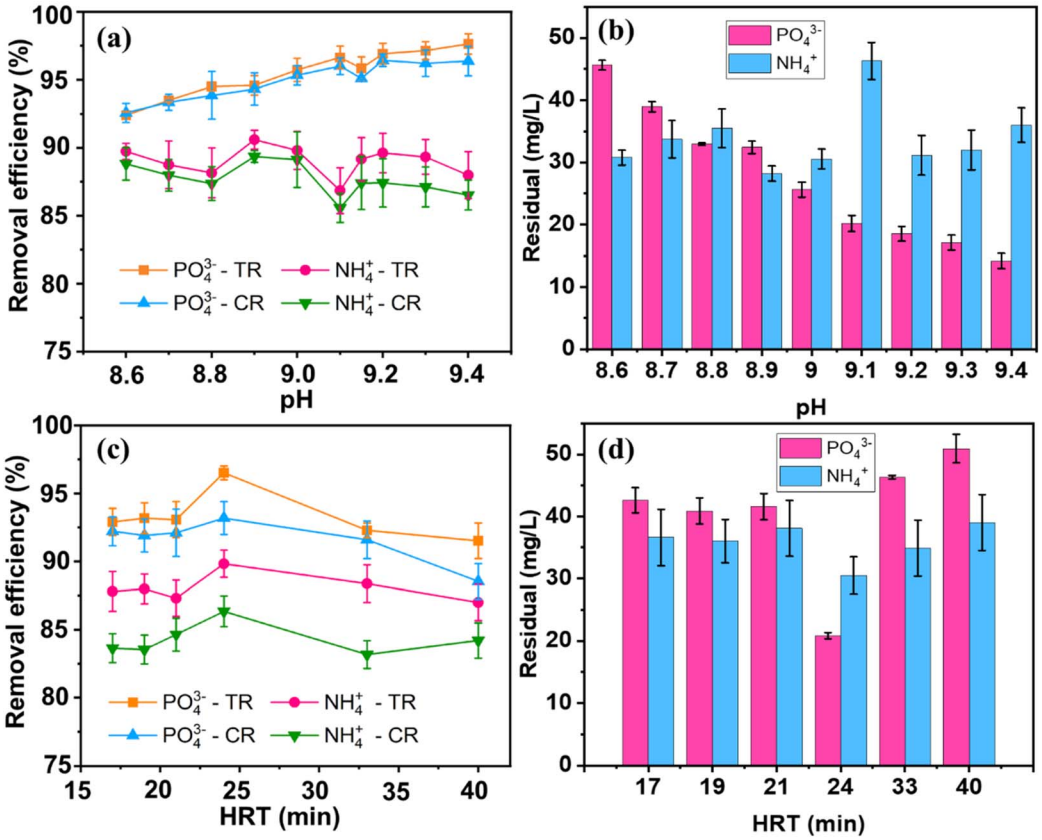

Fig. 2 (a) Effect of pH and (c) hydraulic retention time (HRT) on phosphate and ammonium removal efficiency and (b and d) residual concentrations using the FBHC Process. Error bars represent the standard deviation (±5%) of the replicate experiments.

During the initial 24 minute period, the saturation indices (SI) for magnesium sodium phosphate (Na-struvite, $MgNaPO_4 \cdot 7H_2O$) and struvite were calculated as 1.52 and 2.51, respectively. These values were derived utilizing solubility product constants (K_{sp}) of $10^{-11.6}$ for Na-struvite and $10^{-13.26}$ for struvite,[43] providing preferable thermodynamic conditions for their crystallization. Fig. 2(d) illustrates the residual concentrations of PO_4^{3-} and NH_4^+ after treatment. The residual concentration of PO_4^{3-} decreased to the lowest level of about 20.86 mg L^{-1} at HRT 24 min, corresponding to the highest removal efficiency. The apparent increase in crystallization yield at HRT = 24 min can be explained by the fact that, at this point, the system reaches a hydraulic and reaction steady state, allowing Mg^{2+}, NH_4^+, and PO_4^{3+} ions to effectively interact and crystallize more efficiently. Shorter hydraulic retention times may not be sufficient for crystal nucleation and growth, while longer retention times may lead to partial re-dissolution or dispersion of the formed crystals, thereby reducing the overall yield. Meanwhile, the residual NH_4^+ concentration was approximately 1.5 times higher at 30.51 mg L^{-1}, suggesting that the homogeneous crystallization process in the fluidized bed was more effective in removing phosphate than ammonium. In addition, the presence of other multivalent cations in swine wastewater, which have a strong affinity for phosphate, may promote more efficient phosphate precipitation. The difference in removal efficiency between CR and TR suggests that a portion of both phosphate and ammonium is removed through mechanisms other than crystallization, such as adsorption onto the fluidized bed material surface or other chemical reactions within the system.

3.2.3. Effects of up-flow velocity. The up-flow velocity (U) of the solution in the FBHC process, which is measured in meters per hour (m h^{-1}), represents the linear speed at which the solution moves vertically. This parameter is crucial for optimizing the vulcanization process and designing the most effective reactor. Specifically, for the pellet bed to become fluidized and provide a greater contact area between the pellets and the solution compared to a fixed bed, the up-flow velocity must exceed the minimum fluidization velocity (U_{mf}).[44] The effect of the up-flow velocity on the removal efficiencies of PO_4^{3-} and NH_4^+ was also systematically studied (Fig. 3(a) and (b)). When the up-flow velocity was increased from 14 to 36 m h^{-1}, the recovery efficiencies of PO_4^{3-} and NH_4^+ increased, with CR and TR rising from 95.77 and 95.98% to 96.19 and 96.91% for PO_4^{3-} and from 87.14 and 86.17% to 88.97 and 90.17% for NH_4^+, respectively. Fig. 3(a) also shows relatively large errors for both ions, indicating variability in the crystallization process. NH_4^+ exhibited significant fluctuations across the entire velocity range (14–36 m h^{-1}), whereas PO_4^{3-} showed the most notable variation at higher velocities (29–36 m h^{-1}), suggesting reduced stability of recovery under these conditions. Here, too low an up-flow velocity would not create enough curing for mass

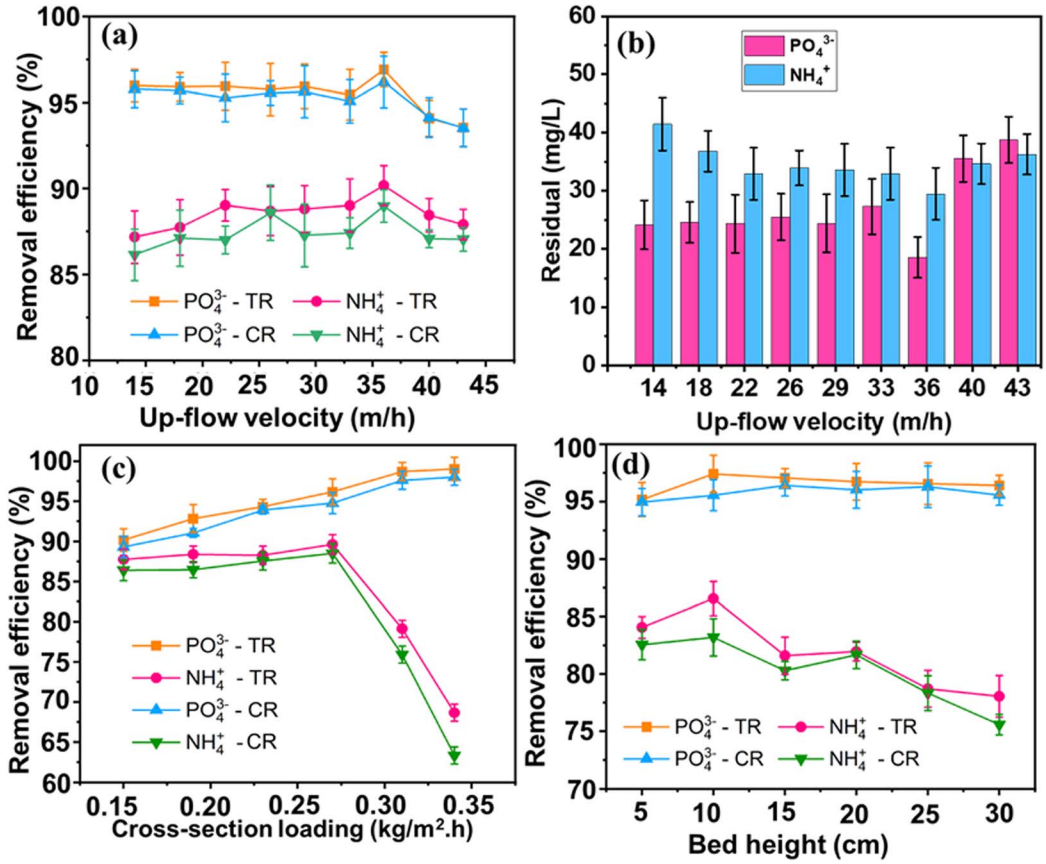

Fig. 3 (a and b) Effect of up-flow velocity, (c) cross-section loading, and (d) bed height on phosphate and ammonium removal efficiency in the FBHC reactor. Error bars represent the standard deviation (±5%) of the replicate experiments.

transfer and thus no granules would form. The improvement of the enhanced up-flow velocity increased the hydraulic movement of the vulcanized pellets, resulting in a higher particle collision frequency and accelerated crystal growth kinetics.[45] However, when the velocity exceeded 36 m h^{-1}, the recovery efficiencies of PO_4^{3-} and NH_4^+ began to decrease gradually with the CR and TR values reaching only 87.04 and 87.9% for NH_4^+ and 93.52 and 93.54% for PO_4^{3-}. The decline in recovery efficiency occurs because once the flow velocity exceeds the optimal threshold, hydraulic energy increases significantly, leading to excessive collisions between crystalline particles. As a result, particle breakage occurs, crystallization efficiency decreases, and nutrient recovery is reduced.[26,46] Therefore, the up-flow velocity was set at 36 m h^{-1} for the subsequent experiments.

3.2.4. Effect of cross-sectional loading. The cross-sectional loading (L) is a key operational parameter commonly utilized to scale up the operation (kg m^{-2} h^{-1}). In this experiment, the cross-sectional loading (L) was adjusted from 0.15 to 0.34 kg m^{-2} h^{-1}, whereas the flow rate of the influent was kept constant at 8 mL min^{-1}. As observed in Fig. 3(c), a cross-sectional loading (L) of 0.27 kg m^{-2} h^{-1} was considered the optimal value in the dolomite seeding system, resulting in a total PO_4^{3-} removal of 96.17% and a crystallization ratio exceeding 94%. However, beyond a loading of 0.27 kg m^{-2} h^{-1}, the phosphate removal efficiency continued to increase slightly and stabilized at a high level (CR 97.99% and TR 99.03%), whereas the ammonium recovery efficiency decreased sharply, falling below 70% at a loading of 0.34 kg m^{-2} h^{-1}. This suggests that at higher cross-sectional loading, certain limiting factors, including reduced residence time and increased shear can inhibit the incorporation of ammonium into struvite. In particular, the formation of smaller struvite particles at higher cross-sectional loading can lead to their leaching, thereby decreasing ammonium recovery. Because phosphorus has a strong tendency to precipitate in struvite, its removal performance may be less affected by the formation and loss of small particles than ammonium.

3.2.5. Effect of bed height. In this work, the effect of the static bed height of homogeneous struvite particles on the removal efficiency of phosphate and ammonium was examined by varying the bed height (5 to 30 cm). The amount of formed particles influences the reactive surface area available for adsorption and further particle formation, thus reducing local supersaturation and the formation of fine particles.[47] A high static bed height promotes solid retention, which can minimize interphase mixing, while a low static bed height favors liquid retention and enhances interphase mixing.[48] As shown in Fig. 3(d), the CR and TR of PO_4^{3-} are significantly higher than those of NH_4^+ when the bed height is adjusted between 5 and 30 cm, and the optimum height was observed to be 10 cm for both PO_4^{3-} and NH_4^+. The variation in results between

replicates was small, especially at a height of 10 cm where the optimum performance was determined. This confirms the important role of the particle bed height and the stability of the FBHC system. Here, the CR and TR of PO_4^{3-} are 95.55 and 97.42%, whereas they are only 83.16 and 86.55% for NH_4^+. However, the CR and TR of NH_4^+ gradually decrease at bed heights above 10 cm. Beyond this height, the elimination efficiency of NH_4^+ declined gradually, possibly owing to reduced mixing or mass transfer limitations. Therefore, a bed height of at least 10 cm is necessary to provide sufficient external surface area to effectively reduce the supersaturation of the incoming magnesium stream (a key component for struvite crystallization) and prevent excessive primary nucleation.[49]

3.2.6. Comparison with modern nutrient recovery methods. To highlight the novelty and technical advantages of the FBHC configuration proposed in this study, the results were compared with advanced nitrogen and phosphorus recovery methods reported in our previous works[4,19] as well as several studies conducted by Kim *et al.*[36] In those earlier studies, fluidized bed crystallization systems were developed to simultaneously recover nutrients from livestock wastewater. However, those configurations still relied on nucleation materials, which could introduce impurities into the crystallized products and reduce the purity of struvite particles. Moreover, key operating factors such as cross-sectional loading, particle bed height, and upflow rate had not been thoroughly investigated, leading to inconsistent crystallization efficiency and variable product morphology. In contrast, the present study employed a seed-free FBHC configuration, coupled with system optimization of several critical operating parameters including pH, residence time, upflow velocity, cross-sectional loading, and bed height. This approach enabled the simultaneous recovery of NH_4^+ and PO_4^{3-} in a single step, achieving high crystallization efficiencies (CR of PO_4^{3-} 95.55% and CR of NH_4^+ 83.18%) and producing particles with uniform size and morphology, which suitable for slow-release fertilizer applications. Compared to the work by Kim *et al.*,[36] which focused solely on struvite crystallization under static batch conditions, the FBHC configuration supports continuous operation and allows precise control of the crystallization process through dynamic and hydraulic adjustments, thereby enhancing system stability and scalability. Additionally, in comparison with electrochemical methods reported in other studies,[13–15] which require specialized equipment and consume large amounts of energy, the FBHC system offers clear advantages in terms of operational simplicity, energy efficiency, low chemical consumption, and minimal sludge generation. These features underscore the high potential of FBHC for practical application in livestock wastewater treatment and nutrient recovery, contributing to the development of a circular economy.

3.3. Characterization of pellets manufactured *via* the FBHC process

The resulting solid products were analyzed employing XRD and SEM techniques. For the jar-tests (conventional precipitation) method, SEM micrographs, as illustrated in Fig. 4(a) and (b), reveal that the formed precipitates consisted of multiple orthorhombic crystals exhibiting trapezoidal or rectangular morphologies with large precipitate particles (0.10–2 mm), rough surfaces, numerous cracks, and voids. In contrast, the sample in Fig. 4(c) had finer but unevenly distributed and easily

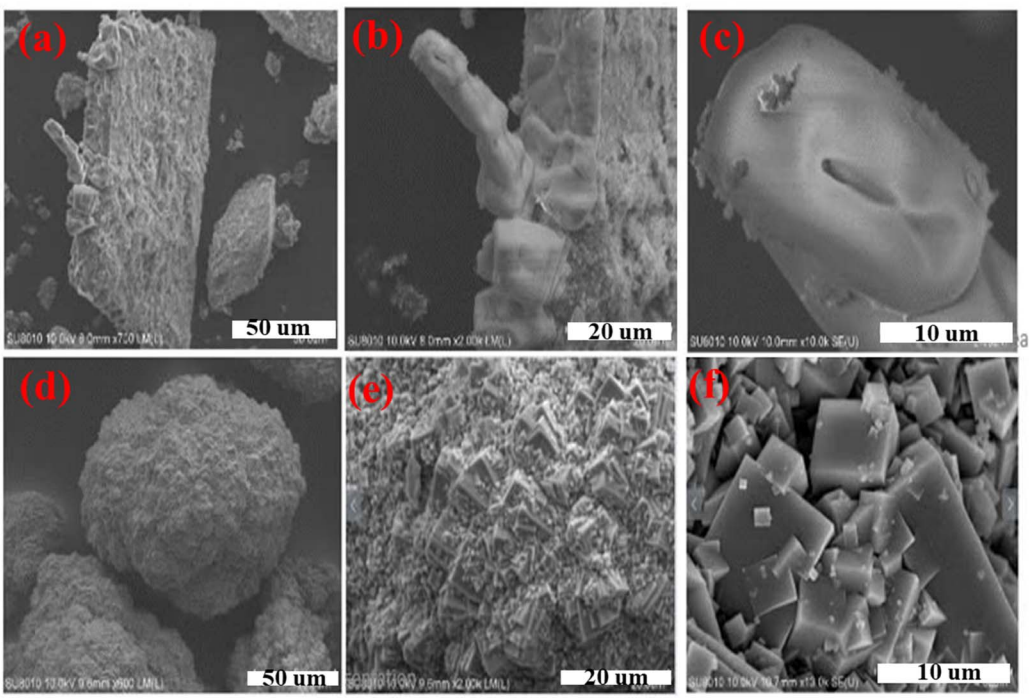

Fig. 4 (a–c) SEM images of the conventional precipitate sample (jar-tests) and (d–f) the sample obtained from the FBHC process.

agglomerated particles. For the FBHC method, SEM observations revealed that the recovered pellets exhibited a homogeneous structure comprising small particles ranging from 0.05 to 1.2 mm with smooth surfaces. Notably, the particles were predominantly spherical (Fig. 4(d)) or oval-shaped (Fig. 4(f)), with uniform size distribution, making them suitable for application as slow-release fertilizers. The XRD patterns presented in Fig. 5 show characteristic peaks at $2\theta = 14.5°$, 16°, 16.7°, 21°, 27°, 29.3°, 30.3°, 32°, 33.5°, 36°, 46.4°, and 51°, consistent with the crystal structure of struvite ($MgNH_4PO_4 \cdot 6H_2O$, JCPDS 15-0762).[50] The obtained struvite product had a purity of 94.3% calculated based on the nitrogen content according to eqn (3). The above results show that the majority of the precipitate mass is pure struvite ($MgNH_4PO_4 \cdot 6H_2O$) with very low impurity content, demonstrating that the crystallization process by the FBHC method is effective and suitable for practical application as slow-release fertilizer. It can be affirmed that the FBHC method stands out for its high recovery efficiency, excellent particle quality, and ease of implementation stemming from precise crystallization control and effective impurity removal.

Based on the particle size distribution diagram obtained from the FBHC process (Fig. 6), a substantial portion of the recovered material consists of fine particles smaller than 0.2 mm, accounting for approximately 40.62% of the total mass. This is followed by fine particles (0.2–0.75 mm) at 31.13%, medium particles (0.75–1.4 mm) at 14.23%, coarse particles (1.4–2 mm) at 7.77%, and very coarse particles (>2 mm) accounting for the smallest fraction at about 6.26%. This distribution suggests that the FBHC process, under the specific conditions applied, tends to produce a majority of fine to very fine particles during P and N recovery. Although the FBHC process is designed to minimize the presence of coarse particles, a small fraction is expected to persist under stable operating conditions. This residual coarse material may contribute to abrasion and fragmentation within the upper section of the system during continuous operation. Particle size plays an important role in the effectiveness of slow release fertilizers. Smaller particles tend to dissolve more quickly, allowing plants to absorb nutrients rapidly, but they are also more susceptible to leaching in highly permeable soils. In contrast, larger particles may dissolve at a slower rate, remaining effective over a longer period while potentially limiting their ability to reach deeper soil layers. As a result, the wide size distribution of the crystalline product obtained from the FBHC system offers a dual advantage by supplying nutrients both immediately and over time, while also reducing nutrient losses through leaching.

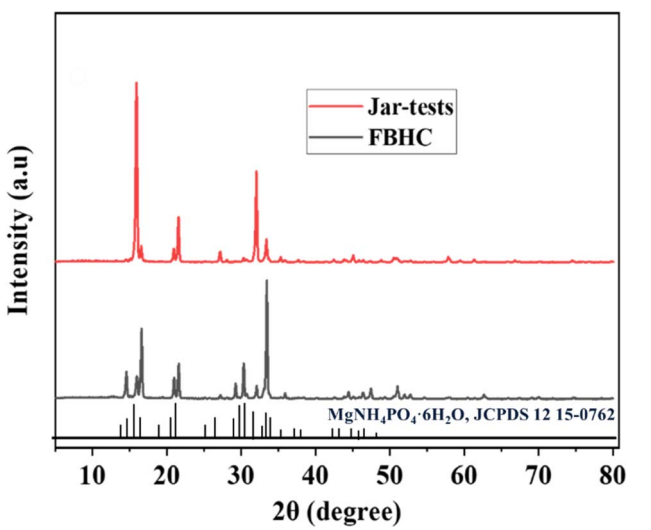

Fig. 5 XRD patterns of the products obtained from jar-tests and FBHC process.

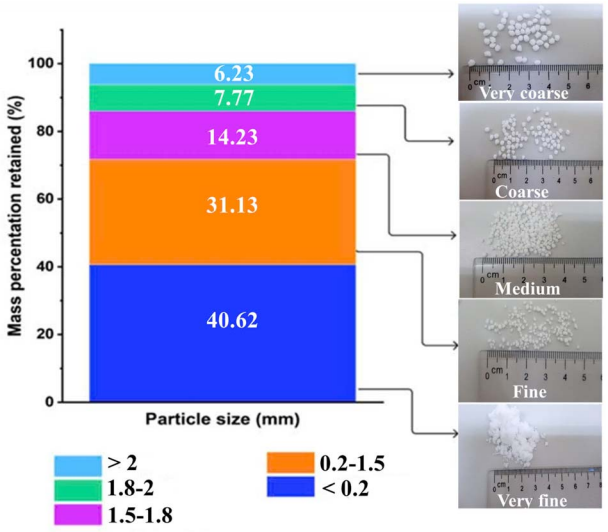

Fig. 6 Particle size distribution of the FBHC-generated pellets.

Fig. 7 depicts SEM images of struvite crystals obtained from the FBHC technique at 250× and 2000× magnifications. The crystals exhibit a well-defined rod-like shape, smooth surfaces, and sharp edges, indicating a high degree of crystallinity. The uniform morphology and absence of abnormal cracks or agglomeration indicate that the precipitation conditions were well controlled, possibly owing to the stability of the fluidized bed and the homogeneous mixing achieved in the FBHC system. The particle sizes are relatively consistent, ranging from 20 μm to 150 μm, which is suitable for applications such as slow-release fertilizers. These morphological characteristics confirm the effectiveness of the FBHC process in producing high-quality struvite crystals.

As shown in Fig. 8, the EDS analysis was applied to determine the elemental composition of the samples. For the FBHC process results, the EDS spectrum showed peaks related to Mg, O, K, P, and Na, suggesting the potential formation of $MgNaPO_4 \cdot 7H_2O$. Nonetheless, the detection of K reveals that potassium ions became incorporated into the crystallized samples, potentially sourced from the initial components in the swine wastewater. This implies a potential involvement of K in the development of complex phosphate precipitates. The presence of a minor quantity of Na indicates the likely formation of a Na-struvite impurity,[51] with the Na^+ ions potentially

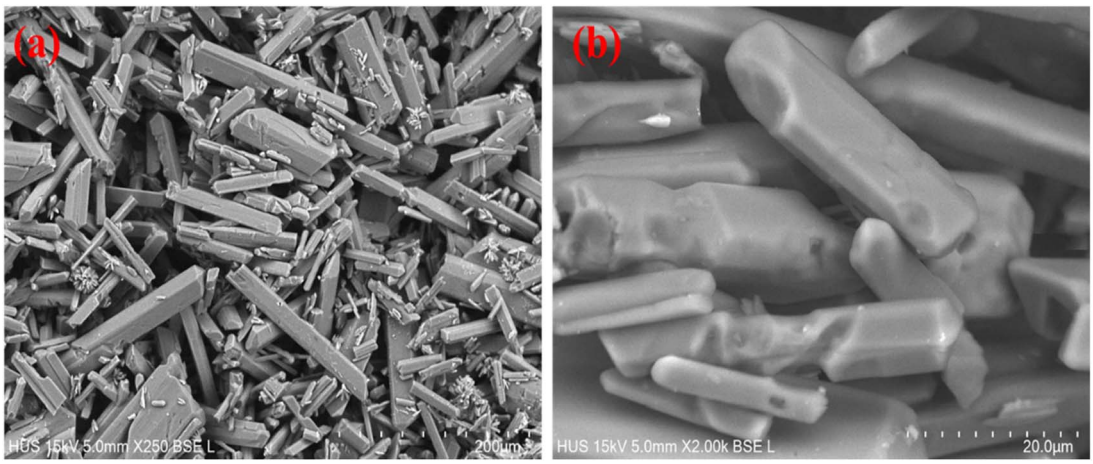

Fig. 7 SEM images of FBHC product (a) ×250 magnification, scale bar = 50 μm; (b) ×2000 magnification, scale bar = 20 μm.

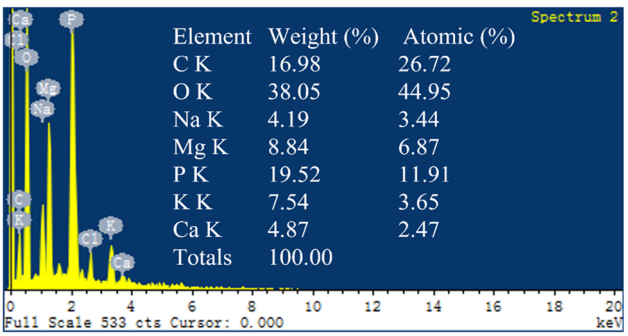

Fig. 8 EDS results of FBHC crystallized pellets after 7 days of operation (struvite pellet formation conditions: pH 9, Mg : P of 1.2, U 36 m h^{-1}, L 0.27 kg m^{-2} h^{-1}, and bed height 10 cm).

originating from the NaOH utilized for pH adjustment. In addition, the theoretical value of struvite for Mg : Na : P : O is 1 : 1 : 1 : 11. However, the experimental result showed that the atomic ratios of Mg : Na : P : O were 1 : 0.5 : 1.7 : 6.5. This deviation may be due to two main reasons. Firstly, during the crystallization of FBHC, it is possible that other precipitates such as $Mg_3(PO_4)_2$ were formed. These precipitate phases have different stoichiometry ratios than struvite, resulting in a change in the measured elemental ratios. Secondly, phosphate ions may have been adsorbed on the surface of the struvite crystals. A higher uptake of phosphorus relative to magnesium on the material's surface will result in an increased phosphorus-to-magnesium ratio as detected by surface EDS.

The struvite particles obtained using FBHC technology in Fig. 9 exhibit a relatively uniform shape, smooth surface, and bright white color, indicating that the crystallization process was effective and the product is of high purity. In Fig. 9(a), the struvite appears evenly distributed without clumping, whereas Fig. 9(b) clearly reveals a nearly spherical structure with small and uniform particle sizes. These observations suggest that the operating conditions in the FBHC system such as pH, ion concentration, and up-flow rate were well controlled, leading to the formation of stable struvite crystals suitable for PO_4^{3-} and NH_4^+ recovery, particularly for use as fertilizer. Although the struvite pellets recovered in this study exhibited high purity, uniform morphology, and an appropriate particle size distribution for use as slow release fertilizers, their actual

Fig. 9 Struvite pellet images from the FBHC process.

effectiveness on plant growth has not been verified. To evaluate the practical application of this product in agricultural production, further studies should focus on bioassays conducted in soil or hydroponic systems. A relevant example is the study by Zabaleta *et al.*,[52] in which almond shell biochar was applied in a soilless *Eruca sativa* cultivation model and can be used as a reference method for assessing the effectiveness of biofertilizers.

4. Conclusions

In summary, the seed-free FBHC technology was successfully developed and applied for the recovery of PO_4^{3-} and NH_4^+ from swine wastewater. Key operational parameters influencing recovery efficiency were systematically optimized. Under the optimal conditions at pH 9, reaction time of 24 min, up-flow velocity of 36 m h^{-1}, cross-sectional loading of 0.27 kg m^{-2} h^{-1}, and 10 cm bed height, the system achieved a TR% of 97.42% for PO_4^{3-} and 86.55% for NH_4^+, with corresponding CR% of 95.55 and 83.18%, respectively. Morphological and particle size analyses indicated that the resulting pellets were predominantly spherical and uniform, with 71.75% of particles measuring below 0.75 mm. The formation of crystalline struvite confirmed the effectiveness of the FBHC process in producing high-purity, homogeneous pellets. These characteristics make the recovered product suitable for use as a slow-release fertilizer in agricultural and horticultural applications. With its high recovery efficiency, low chemical demand, and operational simplicity, FBHC offers strong potential for broader applications in nutrient and resource recovery.

Data availability

Data for this study, including figures and tables are available at article. The data supporting this article have been included as part of the ESI.†

Author contributions

The Anh Luu: methodology, formal analysis, data curation, writing – original draft. Manh Tuan Truong: methodology, writing – review & editing. Gia Cuong Nguyen: writing – review & editing, project administration, formal analysis, data curation. Xuan Thanh Bui: writing – review & editing, methodology. Van Giang Le: writing – review & editing, supervision, project administration, funding acquisition, conceptualization.

Conflicts of interest

The authors declare that they have no known competing financial interests or personal relationships that could have appeared to influence the work reported in this paper.

Acknowledgements

This research was funded by the research project CT05/03-2023-3 of Hanoi Department of Science and Technology, Vietnam. We also thank the editors and anonymous reviewers for their helpful comments and suggestions. We would like to thank Dr Minh Thuan Pham (Cheng Shiu University, Taiwan) for his kind support and helpful suggestions.

References

1 H. Huang, D. Xiao, J. Liu, L. Hou and L. Ding, Recovery and removal of nutrients from swine wastewater by using a novel integrated reactor for struvite decomposition and recycling, *Sci. Rep.*, 2015, **5**(1), 10183.
2 Z.-L. Ye, S.-H. Chen, S.-M. Wang, L.-F. Lin, Y.-J. Yan, Z.-J. Zhang and J.-S. Chen, Phosphorus recovery from synthetic swine wastewater by chemical precipitation using response surface methodology, *J. Hazard. Mater.*, 2010, **176**(1), 1083–1088.
3 Z.-L. Ye, S.-H. Chen, M. Lu, J.-W. Shi, L.-F. Lin and S.-M. Wang, Recovering phosphorus as struvite from the digested swine wastewater with bittern as a magnesium source, *Water Sci. Technol.*, 2011, **64**(2), 334–340.
4 V. G. Le, D. V. N. Vo, C. T. Vu, X. T. Bui, Y. J. Shih and Y. H. Huang, Applying a novel sequential double-column fluidized bed crystallization process to the recovery of nitrogen, phosphorus, and potassium from swine wastewater, *ACS ES&T Water*, 2020, **1**(3), 707–718.
5 M. A. de Boer, L. Wolzak and J. C. Slootweg, Phosphorus: Reserves, Production, and Applications, in *Phosphorus Recovery and Recycling*, ed. H. Ohtake and S. Tsuneda, Springer Singapore, Singapore, 2019, pp. 75–100.
6 C. Numviyimana, J. Warchoł, B. Ligas and K. Chojnacka, Nutrients Recovery from Dairy Wastewater by Struvite Precipitation Combined with Ammonium Sorption on Clinoptilolite, *Mater.*, 2021, **14**(19), 5822.
7 W. G. Harris, A. C. Wilkie, X. Cao and R. Sirengo, Bench-scale recovery of phosphorus from flushed dairy manure wastewater, *Bioresour. Technol.*, 2008, **99**(8), 3036–3043.
8 D. Cândido, A. C. Bolsan, C. E. Hollas, B. Venturin, D. C. Tápparo, G. Bonassa, F. G. Antes, R. L. R. Steinmetz, M. Bortoli and A. Kunz, Integration of swine manure anaerobic digestion and digestate nutrients removal/recovery under a circular economy concept, *J. Environ. Manage.*, 2022, **301**, 113825.
9 H.-D. Ryu, D. Y. Lim, S.-J. Kim, U.-I. Baek, E. G. Chung, K. Kim and J. K. Lee, Struvite Precipitation for Sustainable Recovery of Nitrogen and Phosphorus from Anaerobic Digestion Effluents of Swine Manure, *Sustainability*, 2020, **12**(20), 8574.
10 A. Sendrowski and T. H. Boyer, Phosphate removal from urine using hybrid anion exchange resin, *Desalination*, 2013, **322**, 104–112.
11 J. M. Chimenos, A. I. Fernández, A. Hernández, L. Haurie, F. Espiell and C. Ayora, Optimization of phosphate removal in anodizing aluminium wastewater, *Water Res.*, 2006, **40**(1), 137–143.
12 Q. Guan, Y. Li, Y. Zhong, W. Liu, J. Zhang, X. Yu, R. Ou and G. Zeng, A review of struvite crystallization for nutrient

source recovery from wastewater, *J. Environ. Manage.*, 2023, **344**, 118383.
13 M. E. R. Christiaens, S. Gildemyn, S. Matassa, T. Ysebaert, J. De Vrieze and K. Rabaey, Electrochemical Ammonia Recovery from Source-Separated Urine for Microbial Protein Production, *Environ. Sci. Technol.*, 2017, **51**(22), 13143–13150.
14 W. A. Tarpeh, J. M. Barazesh, T. Y. Cath and K. L. Nelson, Electrochemical Stripping to Recover Nitrogen from Source-Separated Urine, *Environ. Sci. Technol.*, 2018, **52**(3), 1453–1460.
15 X. Chen, Y. Gao, D. Hou, H. Ma, L. Lu, D. Sun, X. Zhang, P. Liang, X. Huang and Z. J. Ren, The Microbial Electrochemical Current Accelerates Urea Hydrolysis for Recovery of Nutrients from Source-Separated Urine, *Environ. Sci. Technol. Lett.*, 2017, **4**(7), 305–310.
16 Z. G. Liu, X. B. Min, F. Feng, X. Tang, W. C. Li, C. Peng, T. Y. Gao, X. L. Chai and C. J. Tang, Development and simulation of a struvite crystallization fluidized bed reactor with enhanced external recirculation for phosphorous and ammonium recovery, *Sci. Total Environ.*, 2021, **760**, 144311.
17 W. A. Tarpeh, K. M. Udert and K. L. Nelson, Comparing Ion Exchange Adsorbents for Nitrogen Recovery from Source-Separated Urine, *Environ. Sci. Technol.*, 2017, **51**(4), 2373–2381.
18 S. K. Pradhan, A. Mikola and R. Vahala, Nitrogen and Phosphorus Harvesting from Human Urine Using a Stripping, Absorption, and Precipitation Process, *Environ. Sci. Technol.*, 2017, **51**(9), 5165–5171.
19 V.-G. Le, D.-V. N. Vo, N.-H. Nguyen, Y.-J. Shih, C.-T. Vu, C.-H. Liao and Y.-H. Huang, Struvite recovery from swine wastewater using fluidized-bed homogeneous granulation process, *J. Environ. Chem. Eng.*, 2021, **9**(3), 105019.
20 Y.-J. Shih, R. R. M. Abarca, M. D. G. de Luna, Y.-H. Huang and M.-C. Lu, Recovery of phosphorus from synthetic wastewaters by struvite crystallization in a fluidized-bed reactor: Effects of pH, phosphate concentration and coexisting ions, *Chemosphere*, 2017, **173**, 466–473.
21 L. Hu, J. Yu, H. Luo, H. Wang, P. Xu and Y. Zhang, Simultaneous recovery of ammonium, potassium and magnesium from produced water by struvite precipitation, *Chem. Eng. J.*, 2020, **382**, 123001.
22 F. C. Ballesteros, A. F. S. Salcedo, A. C. Vilando, Y.-H. Huang and M.-C. Lu, Removal of nickel by homogeneous granulation in a fluidized-bed reactor, *Chemosphere*, 2016, **164**, 59–67.
23 H. P. R. Guevara, F. C. Ballesteros, A. C. Vilando, M. D. G. de Luna and M.-C. Lu, Recovery of oxalate from bauxite wastewater using fluidized-bed homogeneous granulation process, *J. Cleaner Prod.*, 2017, **154**, 130–138.
24 W. D. Scott, T. J. Wrigley and K. M. Webb, A computer model of struvite solution chemistry, *Talanta*, 1991, **38**(8), 889–895.
25 M. L. Salutsky and J. M. Sanborn, Magnesium potassium phosphate-containing fertilizer and process, *US Pat.*, US3285731A, 1966.
26 X. Ye, Z.-L. Ye, Y. Lou, S. Pan, X. Wang, M. K. Wang and S. Chen, A comprehensive understanding of saturation index and upflow velocity in a pilot-scale fluidized bed reactor for struvite recovery from swine wastewater, *Powder Technol.*, 2016, **295**, 16–26.
27 B. B. B. Quedi, F. C. Ballesteros, A. C. Vilando and M.-C. Lu, Recovery of fluoride from wastewater in the form of cryolite granules by fluidized-bed homogeneous crystallization process, *J. Water Process Eng.*, 2024, **66**, 106063.
28 M. S. Rahaman, D. S. Mavinic, A. Meikleham and N. Ellis, Modeling phosphorus removal and recovery from anaerobic digester supernatant through struvite crystallization in a fluidized bed reactor, *Water Res.*, 2014, **51**, 1–10.
29 A. W. Taylor, A. W. Frazier and E. L. Gurney, Solubility products of magnesium ammonium and magnesium potassium phosphates, *Trans. Faraday Soc.*, 1963, **59**, 1580–1584.
30 N. Da Le, T. T. Ha Hoang, V. P. Phung, T. L. Nguyen, T. T. Duong, L. M. Dinh, T. M. Huong Pham, T. X. Binh Phung, T. D. Nguyen, T. N. Duong, T. M. Hanh Le, P. T. Le and T. P. Quynh Le, Trace Metal Element Analysis in Some Seafood in the Coastal Zone of the Red River (Ba Lat Estuary, Vietnam) by Green Sample Preparation and Inductively Coupled Plasma-Mass Spectrometry (ICP-MS), *J. Anal. Methods Chem.*, 2021, **2021**, 6649362.
31 C. T. Vu, C. Lin, C.-C. Shern, G. Yeh, V. G. Le and H. T. Tran, Contamination, ecological risk and source apportionment of heavy metals in sediments and water of a contaminated river in Taiwan, *Ecol. Indic.*, 2017, **82**, 32–42.
32 Warmadewanthi and J. C. Liu, Selective Precipitation of Phosphate from Semiconductor Wastewater, *J. Environ. Eng.*, 2009, **135**(10), 1063–1070.
33 V.-G. Le, C.-T. Vu, Y.-J. Shih, X.-T. Bui, C.-H. Liao and Y.-H. Huang, Phosphorus and potassium recovery from human urine using a fluidized bed homogeneous crystallization (FBHC) process, *Chem. Eng. J.*, 2020, **384**, 123282.
34 I. Çelen and M. Türker, Recovery of Ammonia as Struvite from Anaerobic Digester Effluents, *Environ. Technol.*, 2001, **22**(11), 1263–1272.
35 H. Huang, Y. Chen, Y. Jiang and L. Ding, Treatment of swine wastewater combined with MgO-saponification wastewater by struvite precipitation technology, *Chem. Eng. J.*, 2014, **254**, 418–425.
36 D. Kim, K. J. Min, K. Lee, M. S. Yu and K. Y. Park, Effects of pH, molar ratios and pre-treatment on phosphorus recovery through struvite crystallization from effluent of anaerobically digested swine wastewater, *Environ. Eng. Res.*, 2017, **22**(1), 12–18.
37 H.-D. Ryu, D. Kim and S.-I. Lee, Application of struvite precipitation in treating ammonium nitrogen from semiconductor wastewater, *J. Hazard. Mater.*, 2008, **156**(1), 163–169.
38 E. Banks, R. Chianelli and R. Korenstein, Crystal chemistry of struvite analogs of the type MgMPO4.6H2O (M+ = potassium(1+), rubidium(1+), cesium (1+), thallium(1+), ammonium(1+), *Inorg. Chem.*, 1975, **14**(7), 1634–1639.

39 J. Coppens, R. Lindeboom, M. Muys, W. Coessens, A. Alloul, K. Meerbergen, B. Lievens, P. Clauwaert, N. Boon and S. E. Vlaeminck, Nitrification and microalgae cultivation for two-stage biological nutrient valorization from source separated urine, *Bioresour. Technol.*, 2016, **211**, 41–50.

40 S. Başakçilardan-Kabakci, A. N. İpekoğlu and I. Talinli, Recovery of Ammonia from Human Urine by Stripping and Absorption, *Environ. Eng. Sci.*, 2007, **24**(5), 615–624.

41 K. S. Le Corre, E. Valsami-Jones, P. Hobbs, B. Jefferson and S. A. Parsons, Agglomeration of struvite crystals, *Water Res.*, 2007, **41**(2), 419–425.

42 S. I. Lee, S. Y. Weon, C. W. Lee and B. Koopman, Removal of nitrogen and phosphate from wastewater by addition of bittern, *Chemosphere*, 2003, **51**(4), 265–271.

43 M. Ronteltap, M. Maurer and W. Gujer, Struvite precipitation thermodynamics in source-separated urine, *Water Res.*, 2007, **41**(5), 977–984.

44 K.-Y. Chang, N. N. N. Mahasti and Y.-H. Huang, Fluidized-bed homogeneous crystallization of α-$Al(OH)_3$ for continuous aluminum removal from aqueous solution: Parameter optimization and crystallization mechanism, *J. Water Process Eng.*, 2023, **53**, 103700.

45 K. P. Fattah, D. S. Mavinic and F. A. Koch, Influence of Process Parameters on the Characteristics of Struvite Pellets, *J. Environ. Eng.*, 2012, **138**(12), 1200–1209.

46 C. Zhang, K.-n. Xu, J.-y. Li, C.-w. Wang and M. Zheng, Recovery of Phosphorus and Potassium from Source-Separated Urine Using a Fluidized Bed Reactor: Optimization Operation and Mechanism Modeling, *Ind. Eng. Chem. Res.*, 2017, **56**(11), 3033–3039.

47 V. C. T. Costodes and A. E. Lewis, Reactive crystallization of nickel hydroxy-carbonate in fluidized-bed reactor: Fines production and column design, *Chem. Eng. Sci.*, 2006, **61**(5), 1377–1385.

48 M. M. Bello, A. A. Abdul Raman and M. Purushothaman, Applications of fluidized bed reactors in wastewater treatment – A review of the major design and operational parameters, *J. Cleaner Prod.*, 2017, **141**, 1492–1514.

49 N. N. N. Mahasti, Y.-J. Shih, X.-T. Vu and Y. H. Huang, Removal of calcium hardness from solution by fluidized-bed homogeneous crystallization (FBHC) process, *J. Taiwan Inst. Chem. Eng.*, 2017, **78**, 378–385.

50 C. C. Wang, X. D. Hao, G. S. Guo and M. C. M. van Loosdrecht, Formation of pure struvite at neutral pH by electrochemical deposition, *Chem. Eng. J.*, 2010, **159**(1), 280–283.

51 K. Xu, J. Li, M. Zheng, C. Zhang, T. Xie and C. Wang, The precipitation of magnesium potassium phosphate hexahydrate for P and K recovery from synthetic urine, *Water Res.*, 2015, **80**, 71–79.

52 R. Zabaleta, E. Sánchez, P. Fabani, G. Mazza and R. Rodriguez, Almond shell biochar: characterization and application in soilless cultivation of Eruca sativa, *Biomass Convers. Biorefin.*, 2024, **14**(15), 18183–18200.